Designed amyloid fibers as materials for selective carbon dioxide capture

Dan Li[a,b,c,1], Hiroyasu Furukawa[a,d,1], Hexiang Deng[a,d,2], Cong Liu[a,b,c], Omar M. Yaghi[a,d,3], and David S. Eisenberg[a,b,c,3]

[a]University of California, Los Angeles–Department of Energy Institute for Genomics and Proteomics, and Department of Chemistry and Biochemistry, University of California, Los Angeles, CA 90095; [b]Molecular Biology Institute and [c]Howard Hughes Medical Institute, University of California, Los Angeles, CA 90095; and [d]Department of Chemistry, University of California, Kavli Energy NanoScience Institute at University of California, and Materials Sciences Division, Lawrence Berkeley National Laboratory, Berkeley, CA 94720

Contributed by David Eisenberg, November 20, 2013 (sent for review October 16, 2013)

New materials capable of binding carbon dioxide are essential for addressing climate change. Here, we demonstrate that amyloids, self-assembling protein fibers, are effective for selective carbon dioxide capture. Solid-state NMR proves that amyloid fibers containing alkylamine groups reversibly bind carbon dioxide via carbamate formation. Thermodynamic and kinetic capture-and-release tests show the carbamate formation rate is fast enough to capture carbon dioxide by dynamic separation, undiminished by the presence of water, in both a natural amyloid and designed amyloids having increased carbon dioxide capacity. Heating to 100 °C regenerates the material. These results demonstrate the potential of amyloid fibers for environmental carbon dioxide capture.

amyloid materials | chemisorption | designed fibers

Carbon dioxide has become a focus of scientific attention because of its status as a primary greenhouse gas and the presumed agent of climate change (1, 2). The major sources of anthropogenic carbon dioxide are the flue gas of power plants and automobile emissions. The dominant method for capture is passing postcombustion flue gas through aqueous monoethanolamine (MEA) (3) to form carbamates (4). The industrial MEA process has drawbacks including its requirement for heavy equipment, and the toxic, flammable, corrosive, and volatile nature of MEA (4). More importantly, because of the high heat capacity of aqueous MEA solutions, the energy required for MEA regeneration consumes roughly 30% of the energy output of the power plant (4, 5). To overcome the high energy consumption for MEA regeneration, solid adsorbents such as zeolites, activated carbons, and metal-organic frameworks have been extensively exploited (4, 6–10). These classes of porous materials generally have high capacity and low energy cost for regeneration, but lose their efficiency when exposed to water vapor, as is the case in combustion gases (11, 12). To combine the high affinity of MEA and energy-efficient regeneration of a dry system, new materials with amines implanted in the pores of solid materials are being investigated and show some promise for improved performance (13–15). However, the challenge of selective capture of carbon dioxide remains, especially in the presence of water (16, 17).

Inspired both by the concept of solid-supported amines and by the reversible binding in blood of carbon dioxide by amine groups of hemoglobin, we propose that amyloid fibers containing amine groups may be effective in meeting the challenge stated above. Many proteins and peptides enter the amyloid state, in which they form elongated fibers, with spines consisting of many-stranded β-sheets (18). Amyloid fibers are natural nano-fibers associated with diverse functional and pathological roles. The highly ordered β-strands of amyloid fibers associated by hydrogen-bonding networks and steric-zipper-like interactions confer high stability, insolubility, and stiffness, rendering amyloids useful for the design of functional materials (19–23).

Results

Functionalizing Natural VQIVYK Amyloid Fiber for Carbon Dioxide Capture. In our design of functional amyloid fibers for carbon dioxide capture, we started from a natural hexapeptide VQIVYK, core sequence of the self-association of tau protein (Fig. 1 *A* and *B*) (24). VQIVYK forms amyloid fibers in vitro, and its fibrillar structure shows a typical steric-zipper-like cross-β structure (Fig. 1*C*) (24, 25). In addition, the lysine residue of VQIVYK exposes amino groups on the fiber surface. The ε-amino group of lysine is uncharged at a high pH, and thus capable of forming carbamate with carbon dioxide (26).

We used VQIVYK capped with N-terminal acetylation and C-terminal amidation because it produces higher yields of amyloid fibers than the uncapped peptide (Fig. 1*D*). Mature fibers were collected by centrifugation and lyophilized into a white powder (Fig. 1*E*). The lyophilized material is a mixture containing amyloid fibers and solid buffer components (Table S1), and is stable in air for months. In the following we designate the entire lyophilized fiber material as "fiber material" and the amyloid fiber within the material as "amyloid fiber component."

Strong Interactions Between Carbon Dioxide and VQIVYK Fibers. The VQIVYK fibers are sufficiently open to allow the diffusion of small gaseous molecules, based on nitrogen adsorption isotherm measurements at 77 K (Fig. S1). The profile of the nitrogen isotherm of the fiber material can be classified into type II (27), meaning that the guest molecules are accessible to the fiber matrices in the low-pressure range.

Significance

New and improved materials capable of binding carbon dioxide are essential to addressing the global threat of accelerating climate change. The presently used industrial methods for carbon dioxide capture have severe drawbacks, including toxicity and energy inefficiency. Newer porous materials are so far less effective in water, invariably a component of combustion gases. Here, we present a material for carbon dioxide capture. This material, amyloid fibers in powdered form, selectively captures carbon dioxide in the presence of water and binds carbon dioxide strongly until it is released by heating, regenerating the robust amyloid fibers in an energy efficient process.

Author contributions: D.L., O.M.Y, and D.S.E. designed research; D.L., H.F., H.D., and C.L. performed research; H.F., H.D., C.L., and O.M.Y. contributed new reagents/analytic tools; D.L., H.F., H.D., and C.L. analyzed data; and D.L., H.F., O.M.Y., and D.S.E. wrote the paper.

The authors declare no conflict of interest.

[1]D.L. and H.F. contributed equally to this work.

[2]Present address: College of Chemistry and Molecular Sciences, Wuhan University, Wuhan 430072, China.

[3]To whom correspondence may be addressed. E-mail: yaghi@berkeley.edu or david@mbi.ucla.edu.

This article contains supporting information online at www.pnas.org/lookup/suppl/doi:10.1073/pnas.1321797111/-/DCSupplemental.

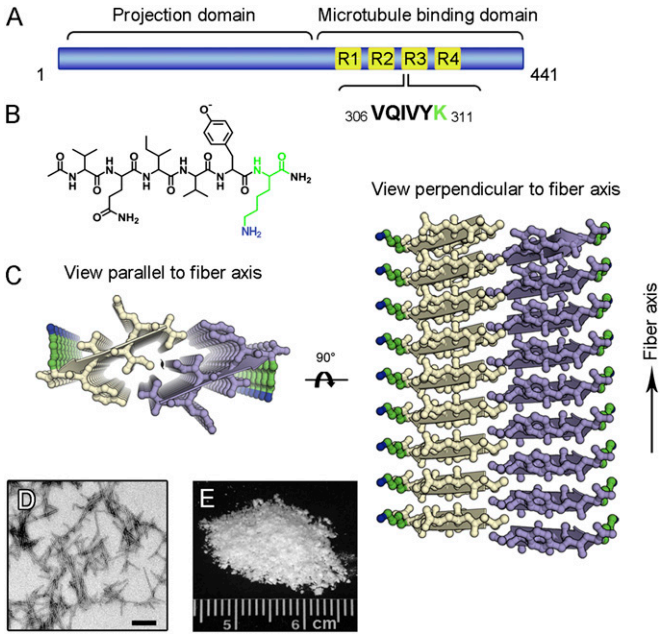

Fig. 1. Structure and fiber formation of VQIVYK. (*A*) Schematic of tau protein, with its repeat regions (R1–R4) in the microtubule binding domain. The hexapeptide VQIVYK (shown with green Lys) derives from R3, functioning in microtubule binding and self-association of tau. (*B*) Chemical structure of capped VQIVYK showing its N-terminal acetylation and C-terminal amidation. (*C*) Crystal structure of uncapped VQIVYK (PDB ID 2ON9). Cartoon arrows represent β-strands. Lysine residues are in green. The ε-amino group of lysine is in blue. The cross-β-spine of the fiber is highly hydrophobic. The pair of sheets pack tightly into a compact "steric zipper" (24, 25). Lysine residues are aligned on the periphery of fiber spine, 4.8 Å apart. (*D*) TEM image of amyloid fibers formed by capped VQIVYK. Scale bar, 300 nm. (*E*) Dry powder of the VQIVYK fiber.

Carbon dioxide binds strongly to VQIVYK amyloid fibers, as shown by adsorption isotherms at 298 K (Fig. 2*A*). The steep initial increase at very low carbon dioxide pressure (<5 Torr) indicates a strong interaction between carbon dioxide and the material (9). After the steep slope region (>10 Torr), the carbon dioxide uptake increases gradually with an increase of pressure, which is similar to typical carbon dioxide physisorption process, and the uptake at 800 Torr reaches 40 $cm^3 \cdot g^{-1}$. The amount of adsorbed carbon dioxide decreases when the carbon dioxide pressure is reduced, whereas the isotherm of fiber material shows hysteresis unlike typical carbon dioxide isotherms. This hysteresis could reflect the strong binding of carbon dioxide with the fiber. Because adsorbed carbon dioxide was not fully desorbed at 10 Torr, the sample was evacuated under the dynamic vacuum (10^{-6} Torr) at room temperature for 24 h. After the evacuation, the carbon dioxide isotherm was recorded to see if carbon dioxide molecules were fully evacuated and strong carbon dioxide binding capacity was recovered. Interestingly, the steep rise of carbon dioxide uptake disappeared (Fig. 2*A*). This implies that carbon dioxide molecules are strongly bound to the VQIVYK fiber so that room-temperature evacuation is not sufficient to liberate carbon dioxide. As a reference, the carbon dioxide isotherm of the sample of solid buffer components was recorded and showed no strong interaction with carbon dioxide.

Spectroscopic Evidence for the Formation of Carbamate. To identify the mechanism of the tight binding of carbon dioxide to VQIVYK fibers, we measured NMR spectra. The fiber material was exposed to ^{13}C labeled carbon dioxide at 1 bar before transferring into a solid-state NMR rotor. Cross-polarization magic-angle-spinning (CP/MAS) ^{13}C NMR spectra of the fibers after ^{13}C carbon dioxide exposure showed a sole strong peak at 163.9 ppm (Fig. 2*B*), whereas peaks arising from fibers are not observed because these carbon atoms are not labeled. Because CP/MAS NMR is not sensitive to floating carbon dioxide, the high-power decoupling (HPDEC) ^{13}C NMR spectrum was also recorded to confirm the absence of free carbon dioxide in the fiber material (Fig. 2*B*). As expected, no signal is detected around 125 ppm (28). Therefore, the NMR peak at 163.9 ppm arises from the carbon which is

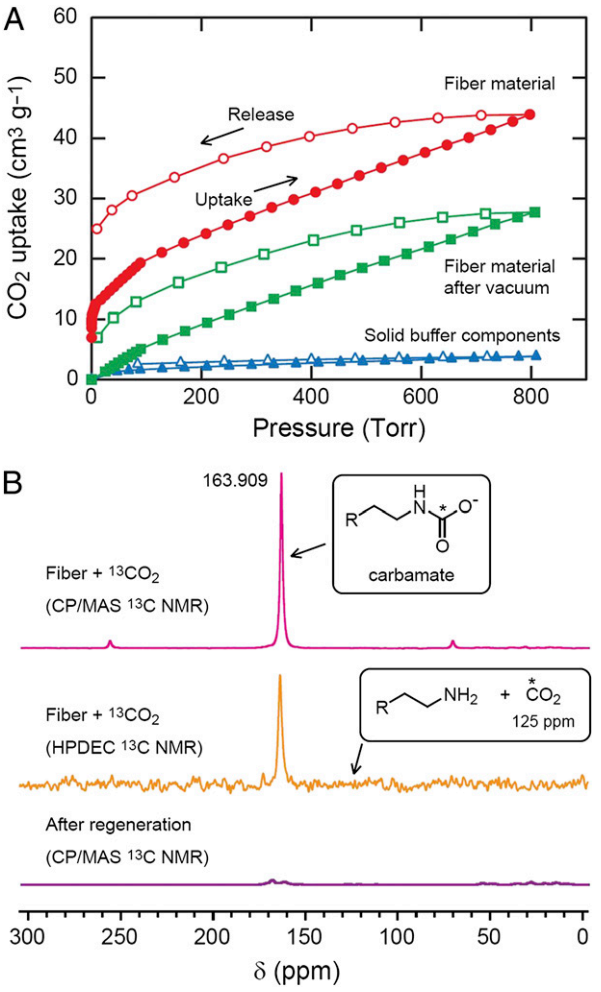

Fig. 2. Mechanism of carbon dioxide adsorption by VQIVYK amyloid fiber material. (*A*) Carbon dioxide adsorption isotherms for VQIVYK fiber material. Solid data points represent gas adsorption and open points are gas desorption after a maximum pressure of ~800 Torr. The steep initial increase of carbon dioxide adsorption by the fiber sample (●) observed at carbon dioxide pressures below 5 Torr indicates a strong interaction between carbon dioxide and the material. The strong adsorption is not recovered by vacuum at room temperature for 24 h (■). The sample of solid buffer components (▲), as a negative control, shows no significant carbon dioxide uptake, confirming that carbon dioxide is mainly adsorbed by fibers in the material. (*B*) Solid-state ^{13}C NMR spectra. An asterisk (*) marks labeled carbon atoms. The CP/MAS ^{13}C NMR spectrum of fiber material with ^{13}C carbon dioxide shows the resonance at 163.909 ppm, ascribed to carbamate. The two subsidiary bands are spinning side bands of the 163.909 band. The HPDEC ^{13}C NMR spectrum of fiber with ^{13}C carbon dioxide shows the absence of the free carbon dioxide signal around 125 ppm, which precludes the possibility of the presence of physisorbed carbon dioxide on the fiber surface. The CP/MAS ^{13}C NMR spectrum of fiber material after regeneration shows that after heating at 100 °C, the carbamate band disappears, indicating a full release of carbon dioxide.

covalently bound to the fiber (28). Indeed, this peak should arise from the formation of carbamate through the reaction of carbon dioxide with the primary amino groups of lysine residues similar to that observed in the amine solutions (4).

Capacity of Carbon Dioxide Chemisorption by the VQIVYK Fiber. The stoichiometry of carbon dioxide binding was estimated by elemental analysis, despite the fiber material being a mixture of VQIVYK peptide and solid buffer components. The fiber material was exposed to carbon dioxide at 1 bar for 1 d before measurement. Table S1 shows the nitrogen–carbon ratio of fiber material before and after carbon dioxide exposure. Assuming that solid buffer components are intact throughout the carbon dioxide sorption measurements, the amount of carbon dioxide sorbed is calculated to be 1.0 ± 0.1 molecules per peptide. Knowing the molecular mass of the peptide (790 $g{\cdot}mol^{-1}$), the molecular mass and molar volume of carbon dioxide, and the proportion of amyloid fibers in the whole material, the 1:1 binding ratio of carbon dioxide and peptide can be converted to ~10 $cm^3{\cdot}g^{-1}$ of carbon dioxide uptake by the fiber material. This value is in good agreement with the carbon dioxide uptake observed in the low-pressure region of the carbon dioxide isotherms (Fig. 2*A*). Usually, carbon dioxide chemisorption gives 2:1 stoichiometry, indicating that two amine molecules capture one carbon dioxide. The unusual 1:1 stoichiometry of carbon dioxide capture by the fiber material is discussed below.

Dynamic Carbon Dioxide Capture Measured by Breakthrough Experiments. For application to environmental stabilization, dynamic separation of carbon dioxide from flue exhausts is more relevant than thermodynamic uptake capacity. To evaluate the dynamic separation capacity of the fiber material, we performed breakthrough experiments which are direct measure of dynamic separation capacity. In these experiments, we mix 16% (vol/vol) of carbon dioxide in a nitrogen gas stream through the material and detect the time of appearance or "breakthrough" of carbon dioxide from the material (10) (Fig. 3, *Inset* and Fig. S2). This percentage is set to mimic the fraction of carbon dioxide in flue gas from power plants (29, 30). The breakthrough curves of fiber material and solid buffer components were recorded. Compared with the solid buffer components, the breakthrough time of the whole fiber material is significantly elongated (Fig. 3). This demonstrates that the majority of carbon dioxide capture arises from the amyloid fiber component in the material rather than from the solid buffer components. Based on the breakthrough curve, the capacity of kinetic carbon dioxide adsorption is estimated to be 0.48 ± 0.15 $mmol_{carbon\ dioxide}{\cdot}g^{-1}$. This number is in reasonable agreement with 0.44 ± 0.10 $mmol_{carbon\ dioxide}{\cdot}g^{-1}$, the thermodynamic carbon dioxide capacity of the whole fiber material calculated from the binding ratio of carbon dioxide to the VQIVYK peptide together with the proportion of the amyloid fiber component in the fiber material. This suggests that carbon dioxide capture by the VQIVYK fiber material is effective for dynamic removal of carbon dioxide from streaming flue gas.

Material Regeneration. During respiration, the reversible carbamate formation of carbon dioxide with hemoglobin is controlled by the local concentration of oxygen (31). For the reversal of the carbamate reaction of amyloid fibers, heating is more practical. Upon heating the material bed to 100 °C under nitrogen flow, carbon dioxide release was detected by the breakthrough system (Fig. S3). The amount of released carbon dioxide calculated by integration of the peak area nearly equals the adsorbed amount of carbon dioxide calculated from the breakthrough time. This finding suggests that 100 °C is sufficient to liberate the carbon dioxide sorbed in the fibers, as carbamates are converted to amino groups. Complete regeneration of the fiber material is further confirmed by disappearance of the carbamate signal on the CP/MAS ^{13}C NMR spectrum after 100 °C heating (Fig. 2*B*). Notice that the carbon dioxide breakthrough curves for three cycles of regeneration are nearly the same (Fig. 3, dry cycles), and the same amount of carbon dioxide is released for each regeneration cycle (Fig. S3). Furthermore, the VQIVYK amyloid fibers maintain their morphology during the process of carbon dioxide adsorption and desorption, as confirmed by transmission electron microscopy (TEM), CP/MAS ^{13}C NMR, and powder X-ray diffraction (Fig. S4).

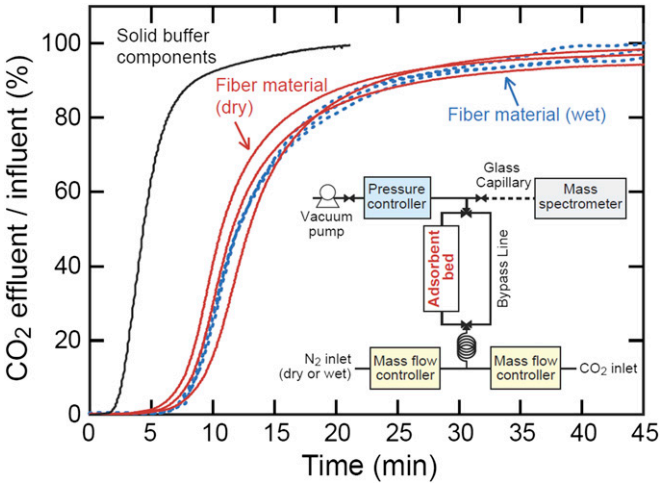

Fig. 3. Breakthrough curves for carbon dioxide sorption by VQIVYK fiber material. Solid lines represent carbon dioxide sorption from the dry gas stream (dry cycles); dotted lines are from gas streams saturated with moisture (wet cycles). The black curve represents solid buffer components; the red and blue curves represent fiber materials. Solid buffer components in the fiber material adsorb carbon dioxide due to its basicity (pH 12). Fiber materials showed an extended breakthrough time compared with the solid buffer components alone, indicating carbon dioxide is mainly adsorbed by the amyloid fiber component. In three dry cycles and three wet cycles of carbon dioxide capture and release, the breakthrough curves are unchanged, indicating that the fiber material is well regenerated in each cycle, and that moisture does not interfere with carbon dioxide capture. The breakthrough time is normalized to 1 g of fiber material. (*Inset*) Schematic illustration of the breakthrough experimental setup.

Carbon Dioxide Capture in the Presence of Water. To examine the performance of the VQIVYK fibers in the presence of water, we tested whether water interferes with carbon dioxide capture by the fibers. We introduced 100% relative humidity into the gas feed stream of the breakthrough experiments. In three cycles of uptake and release in the presence of water, the breakthrough time is sustained (Fig. 3, wet cycles), indicating that water does not change the separation performance of the fiber material on carbon dioxide adsorption in the time period of our recording. In addition, the peptide bonds of VQIVYK remain intact throughout the process even in the presence of water at high pH, as confirmed by mass spectrometry (Fig. S5).

Designed Amyloid Fibers for Increased Carbon Dioxide Binding Capacity. To augment carbon dioxide adsorption, we designed artificial fibers with greater amine density than the natural fiber of VQIVYK. We maintained the fiber spine by keeping residues valine, isoleucine, and tyrosine of positions 1, 3, and 5, but replace or add lysine residues at the other positions (Fig. 4*A*). One of our designs extends the C terminus of the original hexapeptide by one lysine to give the 7mer VQIVYKK. In another design, we mutated the glutamine residue in position 2 to lysine, generating a hexapeptide VKIVYK. The designed peptides both form amyloid fibers with distinctive morphologies under TEM (Fig. 4*A*).

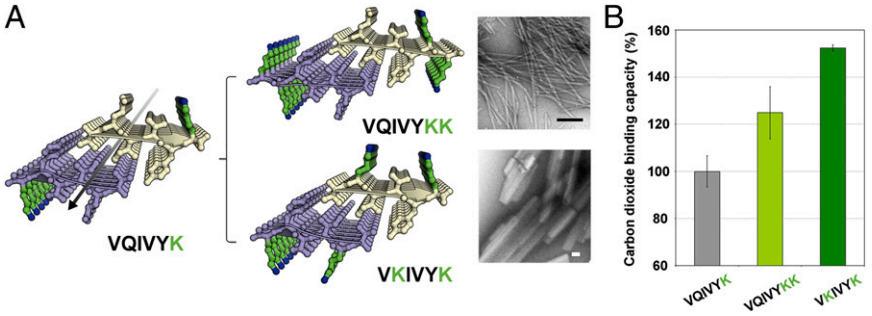

Fig. 4. Designed amyloid fiber materials for increased carbon dioxide capture. (*A*) Structural models and TEM images of VQIVYKK and VKIVYK amyloid fibers. Based on the fiber spine of VQIVYK, VQIVYKK and VKIVYK fibers present more lysines (green)–amino groups for carbon dioxide binding. The black arrow shows the fiber axis. Cartoon arrows represent β-strands. Lysine residues are in green. The ε-amino group of lysine is in blue. Designed peptides form amyloid fibers observed by TEM. Scale bar, 200 nm. (*B*) With the increased numbers of amino groups, VQIVYKK and VKIVYK fibers show significantly higher carbon dioxide binding capacity than the original VQIVYK fiber.

Breakthrough experiments proved that the engineered fibers have significantly increased carbon dioxide binding capacity by up to 55% compared with that of the natural fiber of VQIVYK (Fig. 4*B*). Notice that although there is double the number of amines in the designed fibers, we do not observe a twofold increase in binding capacity, indicating that in these fibers amines are only partially accessible and reactive. Future fiber designs will further augment the capacity.

Discussion

The reaction of carbon dioxide with a primary alkanolamine to form carbamate proceeds in two steps:

$$RNH_2 + CO_2 \rightleftharpoons RNH_2^+COO^-, \quad [1]$$

$$RNH_2^+COO^- + B \rightleftharpoons RNHCOO^- + BH^+. \quad [2]$$

B represents base in Eq. **2**. The first step (Eq. **1**) is the rate-determining step, but carbamic acid is not stable. The reaction rapidly proceeds to form carbamate in the presence of base (Eq. **2**). In conventional amine solutions, the base is a second amine molecule; thus two amines capture one carbon dioxide (32, 33). In amyloid fiber materials, we observed 1:1 stoichiometry where one amine binds to one carbon dioxide. We hypothesize that, rather than amines, buffer salts act as the base, which is supported by experiments with different buffer systems (Fig. S6). The results show that removal of buffer salts at pH 10.8, a pH at which half of lysine side chains (pK_a = 10.8) are protonated and cannot act as base, caused complete loss of chemisorption.

Buffer salts may also postpone the protonation of amines when water presents in the gas stream. Carbon dioxide and water form carbonic acid, although with less than 1% of the dissolved carbon dioxide (26), which protonates amines, thereby reducing their formation of carbamate. Buffer salts in the fiber material are stronger bases than the amines and preferentially accept protons, thereby protecting amines from inactivation. As seen in dynamic adsorption in the presence of water (Fig. 3), the carbon dioxide capacity is not diminished in three cycles of capture and release.

Reminiscent of the vast array of functions exhibited by natural proteins, amyloid fibers as materials offer a general solid platform on which designed functionalities can be readily realized by varying the amino acid sequence of the peptide units. Applications of amyloid fibers have been explored in the fields including conductive nanowires (34), nanostructured protein films (35), light-harvesting nano-device (36, 37), and retroviral gene transfer boosting (38). The properties demonstrated here of amyloid fibers for carbon dioxide capture fall short of those needed in a practical material operating in the demanding conditions of water, acid, and temperature of flue gas. Also, the adsorption capacity of our best current fiber material (0.5–0.7 mmol·cm^{-3}) is significantly below that of MEA solution (~3 mmol·cm^{-3}) (10). However, as a solid material, amyloid fibers show many favorable properties including (*i*) relatively mild regeneration temperature (100 °C), (*ii*) high structural rigidity and thermal stability, especially for peptide fibers, as opposed to amyloid fibers of full proteins (37, 39), (*iii*) compatible with the presence of water, (*iv*) stable in air, and (*v*) readily self-assembling from peptides, enabling easy manufacture. Furthermore, it is expected that (*i*) bacterial production of amyloid peptides offers potential cost savings over chemical synthesis, and genetic methods of tuning functionality, and (*ii*) amyloid fibers are potentially biodegradable, with little harm to the environment. Therefore, further optimization of designed amyloid fibers for carbon dioxide capture is worth pursuing.

Materials and Methods

Amyloid Fiber Preparation. All peptides were custom synthesized by Celtek Peptides and were used as received as a TFA salt. Purity was over 98% (wt/wt) by HPLC. The peptides were N-terminally acetylated and C-terminally amidated for high yields of amyloid fibers. VQIVYK fibers were formed in the solution containing 1 mM VQIVYK, 50 mM sodium phosphate buffer, pH 12.0. VQIVYKK fibers were formed in the solution containing 5 mM VQIVYKK, 50 mM sodium phosphate buffer, 0.2 M sodium chloride, pH 8.0. VKIVYK fibers were formed in the solution containing 1 mM VKIVYK, 50 mM sodium phosphate buffer, 0.2 M sodium chloride, pH 8.0. All fiber-forming solutions were incubated at 37 °C with agitation for 7–10 d. Fiber formation was monitored by TEM. Fibers were collected by centrifugation at 36,320 × *g* for 20 min, and were resuspended with 50 mM sodium phosphate buffer, pH 12, to keep the ε-amino group of lysine in the dissociated state. The fiber suspension was lyophilized until the sample became a white powder. The lyophilized fibers were stored in air-tight containers at room temperature. The sample of solid buffer components, used as negative control, was lyophilized 50 mM sodium phosphate buffer, pH 12.

TEM. Five μL of each sample were spotted directly onto freshly glow-discharged carbon-coated electron microscopy grids (Ted Pella). After 3-min incubation, grids were rinsed twice with 5 μL distilled water and stained with 1% uranyl acetate for 1 min. Specimens were examined in a JEM1200-EX electron microscope at an accelerating voltage of 80 kV. Images were recorded digitally by wide-angle (top mount) BioScan 600W 1 × 1K digital camera (Gatan).

Gas Adsorption Measurements. Nitrogen and carbon dioxide isotherms were collected on a Quantachrome Autosorb-1 automatic volumetric gas adsorption analyzer. The samples were outgassed to 10^{-6} Torr. Ultrahigh-purity-grade nitrogen, He (99.999% purity), and carbon dioxide gases (99.995% purity) were used throughout the adsorption experiments.

Solid-State NMR. High-resolution solid-state NMR spectra were recorded at ambient temperature on a Bruker DSX-300 spectrometer using a standard Bruker magic-angle-spinning (MAS) probe with 4-mm (outside diameter) zirconia rotors. CP/MAS was used to acquire ^{13}C data at 75.47 MHz. The ^{1}H and ^{13}C 90° pulse widths were both 4 μs. The CP contact time was varied between 1.5 and 5 ms. High-power two-pulse phase modulation ^{1}H decoupling was applied during data acquisition. The decoupling frequency corresponded to 72 kHz. The MAS sample spinning rate was 10 kHz. Recycle delays for CP/MAS between scans varied between 3 and 20 s, depending upon the compound as determined by observing no apparent loss in the ^{13}C signal intensity from one scan to the next. The ^{13}C chemical shifts are given relative to tetramethylsilane as 0 ppm, calibrated using the methylene carbon signal of adamantane assigned to 37.77 ppm as a secondary reference. HPDEC ^{13}C spectrum was measured on a stationary rotor without magic angle spinning.

Before exposure to ^{13}C carbon dioxide, the sample was outgassed in a glass vial with Mityvac hand vacuum pump (Nalgene). ^{13}C carbon dioxide (Sigma-Aldrich, 99 atom % ^{13}C; <3 atom % ^{18}O) was then injected into the vial at 1 bar for 1 d. The sample was then transferred to zirconia NMR rotors right before the NMR measurement.

Elemental Analysis. Elemental analysis was carried out on a Thermo Scientific FLASH 2000 Series CHNS/O Analyzer. For each measurement 2–3 mg of sample was used. More than three measurements were performed on each fiber sample to guarantee accuracy.

Breakthrough Experiments. A laboratory-made breakthrough system was used to evaluate dynamic carbon dioxide selectivity over nitrogen. Adsorbent materials were packed in stainless steel Swagelok tubing (4 mm i.d. × 50 mm). Volume not occupied by the adsorbent bed was filled with glass beads (Sigma, 150–212 μm). The gas feed stream was a 16% (vol/vol) mixture of carbon dioxide in nitrogen for separation, and 100% (vol/vol) nitrogen for regeneration, which were determined by MKS Alta digital mass flow controllers. The pressure was held at 760 Torr by an MKS type 640 pressure controller. The gaseous effluent from the sample bed was monitored for carbon dioxide, nitrogen, water, and oxygen by using a mass spectrometer (Hiden Analytical HPR20).

In wet cycles, nitrogen in the gas feed steam was saturated with moisture by passing through humidifying cells (Glassblowers.com Inc.). The humidifying cells sit in a water bath of 30 °C generating 100% relative humidity, which is equivalent to ~3% (vol/vol) of moisture. Before introducing carbon dioxide into the gas feed stream, the amyloid material was equilibrated with 100% moisture-saturated nitrogen for 2 h. In the process of regeneration, the material bed was heated to 100 °C as in dry cycles, but purged with nitrogen saturated with moisture.

Powder X-Ray Diffraction. Powder X-ray diffraction was performed on a Bruker D8 Discover θ–θ diffractometer in reflectance Bragg–Brentano geometry at 40 kV, 40 mA (1,600 W) for Cu $K\alpha_1$ radiation ($\lambda = 1.5406$ Å).

Matrix-Assisted Laser Desorption Ionization Time-of-Flight Mass Spectrometry. Matrix-assisted laser desorption ionization time-of-flight (MALDI-TOF) mass spectra were acquired on the Voyager-DE STR Biospectrometry Workstation equipped with a nitrogen laser. Measurements were performed in the positive ion mode. Before MALDI mass analysis, samples were mixed with 0.5 μL of 10 mg mL^{-1} 2,5-dihydroxybenzoic acid in water–acetonitrile (70:30) solution on a stainless steel target plate and allowed to dry in a vacuum chamber. Data were collected in reflection mode using an accelerating voltage of 25 kV and a delay time of 200 ns. The accumulated spectra shown were obtained by 200–800 laser shots.

Fiber Spine Modeling. The model of VQIVYKK was generated using the crystal structure of VQIVYK [Protein Data Bank (PDB) ID 2ON9] as a template. The C terminus was extended by one residue using ideal beta strand phi–psi angles. The C-terminal residues were mutated to lysine side chains. Rotamers were selected to avoid steric clash. Modeling was performed using the program COOT (40). The model was illustrated using Pymol (41). The model of VKIVYK was created in a similar way.

ACKNOWLEDGMENTS. We thank D. Anderson, University of California, Los Angeles (UCLA) for technical support and discussion, M. Sawaya (UCLA) for structure modeling, S. Das (UCLA) for his initial work, and C. Stevens (University of California, Berkeley) for her help in elemental analysis. This work was supported by Department of Energy BER Grant DE-FC03-02ER63421, National Science Foundation Grant MCB-0958111, and Howard Hughes Medical Institute.

1. Pachauri RK, Reisinger A, eds (2008) *Climate Change 2007: Synthesis Report* (IPCC, Geneva, Switzerland).
2. Song C (2006) Global challenges and strategies for control, conversion and utilization of CO_2 for sustainable development involving energy, catalysis, adsorption and chemical processing. *Catal Today* 115(1-4):2–32.
3. Aaron D, Tsouris C (2005) Separation of CO_2 from flue gas: A review. *Sep Sci Technol* 40(1-3):321–348.
4. Sumida K, et al. (2012) Carbon dioxide capture in metal-organic frameworks. *Chem Rev* 112(2):724–781.
5. Yang H, et al. (2008) Progress in carbon dioxide separation and capture: A review. *J Environ Sci (China)* 20(1):14–27.
6. An J, Fiorella RP, Geib SJ, Rosi NL (2009) Synthesis, structure, assembly, and modulation of the CO_2 adsorption properties of a zinc-adeninate macrocycle. *J Am Chem Soc* 131(24):8401–8403.
7. Millward AR, Yaghi OM (2005) Metal-organic frameworks with exceptionally high capacity for storage of carbon dioxide at room temperature. *J Am Chem Soc* 127(51): 17998–17999.
8. Llewellyn PL, et al. (2008) High uptakes of CO_2 and CH_4 in mesoporous metal-organic frameworks MIL-100 and MIL-101. *Langmuir* 24(14):7245–7250.
9. Gassensmith JJ, et al. (2011) Strong and reversible binding of carbon dioxide in a green metal-organic framework. *J Am Chem Soc* 133(39):15312–15315.
10. Britt D, Furukawa H, Wang B, Glover TG, Yaghi OM (2009) Highly efficient separation of carbon dioxide by a metal-organic framework replete with open metal sites. *Proc Natl Acad Sci USA* 106(49):20637–20640.
11. Low JJ, et al. (2009) Virtual high throughput screening confirmed experimentally: porous coordination polymer hydration. *J Am Chem Soc* 131(43):15834–15842.
12. Kaye SS, Dailly A, Yaghi OM, Long JR (2007) Impact of preparation and handling on the hydrogen storage properties of Zn_4O(1,4-benzenedicarboxylate)$_3$ (MOF-5). *J Am Chem Soc* 129(46):14176–14177.
13. Jadhav PD, et al. (2007) Monoethanol amine modified zeolite 13X for CO_2 adsorption at different temperatures. *Energy Fuels* 21(6):3555–3559.
14. Hicks JC, et al. (2008) Designing adsorbents for CO_2 capture from flue gas-hyperbranched aminosilicas capable of capturing CO_2 reversibly. *J Am Chem Soc* 130(10): 2902–2903.
15. Xu X, Song C, Andrésen J, Miller BG, Scaroni AW (2003) Preparation and characterization of novel CO_2 "molecular basket" adsorbents based on polymer-modified mesoporous molecular sieve MCM-41. *Microporous Mesoporous Mater* 62(1-2):29–45.
16. Li G, Xiao P, Webley PA, Zhang J, Singh R (2009) Competition of CO_2/H_2O in adsorption based CO_2 capture. *Energy Procedia* 1(1):1123–1130.
17. Nugent P, et al. (2013) Porous materials with optimal adsorption thermodynamics and kinetics for CO_2 separation. *Nature* 495(7439):80–84.
18. Eisenberg D, Jucker M (2012) The amyloid state of proteins in human diseases. *Cell* 148(6):1188–1203.
19. Makin OS, Atkins E, Sikorski P, Johansson J, Serpell LC (2005) Molecular basis for amyloid fibril formation and stability. *Proc Natl Acad Sci USA* 102(2):315–320.
20. Hirota-Nakaoka N, Hasegawa K, Naiki H, Goto Y (2003) Dissolution of β_2-microglobulin amyloid fibrils by dimethylsulfoxide. *J Biochem* 134(1):159–164.
21. Knowles TP, et al. (2007) Role of intermolecular forces in defining material properties of protein nanofibrils. *Science* 318(5858):1900–1903.
22. Knowles TP, Buehler MJ (2011) Nanomechanics of functional and pathological amyloid materials. *Nat Nanotechnol* 6(8):469–479.
23. Gazit E (2007) Self-assembled peptide nanostructures: The design of molecular building blocks and their technological utilization. *Chem Soc Rev* 36(8): 1263–1269.
24. Sawaya MR, et al. (2007) Atomic structures of amyloid cross-β spines reveal varied steric zippers. *Nature* 447(7143):453–457.
25. Nelson R, et al. (2005) Structure of the cross-β spine of amyloid-like fibrils. *Nature* 435(7043):773–778.
26. Edsall JT, Wyman J (1958) *Biophysical Chemistry* (Academic, New York), Vol 1.
27. Lowell S, Shields JE, Thomas MA, Thommes M (2004) *Characterization of Porous Solids and Powders: Surface Area, Pore Size and Density* (Kluwer, Dordrecht, The Netherlands).
28. Pinto ML, Mafra L, Guil JM, Pires J, Rocha J (2011) Adsorption and activation of CO_2 by amine-modified nanoporous materials studied by solid-state NMR and $^{13}CO_2$ adsorption. *Chem Mater* 23(6):1387–1395.
29. Figueroa JD, Fout T, Plasynski S, Mcllvried H, Srivastava RD (2008) Advances in CO_2 capture technology-The U.S. Department of Energy's carbon sequestration program. *Int J Greenh Gas Control* 2(1):9–20.
30. Hudson MR, et al. (2012) Unconventional, highly selective CO_2 adsorption in zeolite SSZ-13. *J Am Chem Soc* 134(4):1970–1973.
31. Nelson DL, Cox MM (2008) *Lehninger Principles of Biochemistry* (Freeman, New York), 5th Ed.
32. Caplow M (1968) Kinetics of carbamate formation and breakdown. *J Am Chem Soc* 90(24):6795–6803.

33. Mimura T, Suda T, Iwaki I, Honda A, Kumazawa H (1998) Kinetics of reaction between carbon dioxide and sterically hindered amines for carbon dioxide recovery from power plant flue gases. *Chem Eng Commun* 170(1):245–260.
34. Scheibel T, et al. (2003) Conducting nanowires built by controlled self-assembly of amyloid fibers and selective metal deposition. *Proc Natl Acad Sci USA* 100(8):4527–4532.
35. Knowles TP, Oppenheim TW, Buell AK, Chirgadze DY, Welland ME (2010) Nanostructured films from hierarchical self-assembly of amyloidogenic proteins. *Nat Nanotechnol* 5(3):204–207.
36. Channon KJ, Devlin GL, MacPhee CE (2009) Efficient energy transfer within self-assembling peptide fibers: A route to light-harvesting nanomaterials. *J Am Chem Soc* 131(35):12520–12521.
37. Fitzpatrick AW, Park ST, Zewail AH (2013) Exceptional rigidity and biomechanics of amyloid revealed by 4D electron microscopy. *Proc Natl Acad Sci USA* 110(27): 10976–10981.
38. Yolamanova M, et al. (2013) Peptide nanofibrils boost retroviral gene transfer and provide a rapid means for concentrating viruses. *Nat Nanotechnol* 8(2): 130–136.
39. Baldwin AJ, et al. (2011) Metastability of native proteins and the phenomenon of amyloid formation. *J Am Chem Soc* 133(36):14160–14163.
40. Emsley P, Cowtan K (2004) Coot: Model-building tools for molecular graphics. *Acta Crystallogr D Biol Crystallogr* 60(Pt 12 Pt 1):2126–2132.
41. The PyMOL Molecular Graphics System, Version 1.5.0.4 (Schrödinger, LLC, Portland OR).